Wind and Structures, *Vol. 20, No. 4 (2015) 509-525*
DOI: http://dx.doi.org/10.12989/was.2015.20.4.509

Effect of noise barrier on aerodynamic performance of high-speed train in crosswind

Hai Zhao[1a], Wanming Zhai[*2] and Zaigang Chen[2b]

[1]*Qingdao Sifang Rolling Stock Research Institute Co., Ltd., Qingdao 266031, P. R. China*
[2]*Train and Track Research Institute, State Key Laboratory of Traction Power, Southwest Jiaotong University, Chengdu 610031, P. R. China*

(Received October 8, 2014, Revised January 13, 2015, Accepted January 23, 2015)

Abstract. A three-dimensional aerodynamic model and a vehicle dynamics model are established to investigate the effect of noise barrier on the dynamic performance of a high-speed train running on an embankment in crosswind in this paper. Based on the developed model, flow structures around the train with and without noise barrier are compared. Effect of the noise barrier height on the train dynamic performance is studied. Then, comparisons between the dynamic performance indexes of the train running on the windward track and on the leeward track are made. The calculated results show that the noise barrier has significant effects on the structure of the flow field around the train in crosswind and thus on the dynamic performance of the high-speed train. The dynamic performance of the train on the windward track is better than that on the leeward track. In addition, various heights of the noise barrier will have different effects on the train dynamic performance. The dynamic performance indexes keep decreasing with the increase of the noise barrier height before the height reaches a certain value, while these indexes have an inverse trend when the height is above this value. These results suggest that optimization on the noise barrier height is possible and demonstrate that the designed noise barrier height of the existing China Railway High-speed line analysed in this article is reasonable from the view point of the flow field structure and train dynamic performance although the noise barrier is always designed based on the noise-related standard.

Keywords: high-speed railway; noise barrier; crosswind; train dynamic performance; aerodynamics

1. Introduction

With the rapid development of high-speed railway and the increase of train speed, the running safety and ride comfort of high-speed train are concerned increasingly. This is because serious vehicle accidents, such as overturning, derailment and side slipping, may occur in the extremely windy environments. These serious problems which are urgently demanded to be solved have promoted the fast development in the research on the train aerodynamics, especially for the high-speed trains.

Baker (1991) established a universal analytical framework based on the analysis of the steady

∗Corresponding author, Professor, E-mail: wmzhai@swjtu.edu.cn
[a] R&D Engineer, E-mail: zhao.hai@outlook.com
[b] Associate Professor, E-mail: zgchen@home.swjtu.edu.cn

http://www.techno-press.org/?journal=was&subpage=8 ISSN: 1226-6116 (Print), 1598-6225 (Online)

and unsteady aerodynamic forces of different trains in crosswind condition, and a number of wind tunnel experiments were carried out to validate the analytical framework. Khier *et al.* (2000) investigated the flow field characteristics around a train under different yaw angles of wind based on a simplified model with high Reynolds number by applying the Reynolds-averaged Navier-Stokes (RANS) combined with k-ε turbulence model. The results indicated that different flow structures were found under different yaw angles. Li and Tian (2012) simulated flow fields around double-deck container vehicles with different structures and obtained the critical speed with steady RANS k-ε model. Gilbert *et al.* (2013) carried out a research work to study the transition of the pressure-loading patterns from unconfined to enclosed spaces, where the transitions from the open air to single and double vertical walls, partially enclosed spaces, short single-track tunnels and a longer tunnel are taken into consideration. Rezvani and Mohebbi (2014) explored the unsteady aerodynamic performance of crosswind around the ATM train under different yawing conditions by employing the three-dimensional RANS equations. Hemida (2006) carried on a LES for the flow structure around simplified high-speed trains in side wind. Sun *et al.* (2013) studied the dynamic characteristics of a high-speed train in crosswind by using the software of SIMPACK. Dierichs *et al.* (2007) investigated the flow field around ICE3 tractor running on a 6 m embankment by experiment and numerical simulation. The numerical and experimental results were consistent with each other, indicating that the aerodynamic performance of the vehicle running on leeward track was worse than that on windward track. And recently, Herbsta *et al.* (2014) introduced some aerodynamic prediction tools for high-speed trains.

These techniques for the aerodynamic simulation are also employed to the train-bridge coupled dynamic systems. Xia *et al*. (2008) studied the dynamic response of the bridge, the running safety and stability of the train under the action of wind based on a wind–train–bridge system model. Zhang *et al.* (2013) carried out the analysis on the effect of wind barriers on the running safety of trains on bridge under the turbulent cross wind condition based on the vehicle-bridge dynamic interaction system. Guo *et al.* (2013) developed a three-dimensional wind–train–bridge interaction model by integration of a spatial finite element bridge model, a train model, and a turbulent wind model, and they applied this model to study the running safety of the train on the Tsing Ma Bridge which was subjected to Typhoon York. By their study, the permitted train speed under different wind velocities could be obtained. Li *et al.* (2014) measured the aerodynamic forces and moments acting on the moving vehicle model on the bridge deck in crosswinds by wind tunnel test, where the influences of the vehicle speed, wind yaw angle, rail track position and vehicle type were considered.

Noise barrier is widely used in high-speed railways worldwide in order to prevent propagation of noise induced by high-speed train. In China, noise barrier is setup for noise reduction on several high-speed railways, such as Beijing–Shanghai high-speed railway, Beijing–Tianjin intercity railway and Beijing–Guangzhou high-speed railway. In crosswind, noise barrier also acts as a windbreak wall and trains are protected to a certain extent. Meanwhile, noise barrier could change the flow structure around train and affect the aerodynamic performance, which is likely to change the dynamic performance of the high-speed train, or even cause serious accidents, e.g., derailment and overturning. Hence, further study on the effect of noise barrier on the dynamic performance of high-speed train is necessary. However, few papers focusing on this problem are found due to its complexity. Khier *et al.* (2002) simulated the flow structure around train running on an embankment equipped with single side noise barrier in crosswind and the result showed that the aerodynamic forces and moments acting on train decreased when the noise barrier was equipped. Luo and Yang (2010) studied the effect of the noise barrier height on the aerodynamic performance

of a train running on a viaduct.

It can be seen that most of these studies were concentrated on the effect of the noise barrier on the high-speed train aerodynamic characteristics. In practice, change of the flow field structure due to the setting up of the noise barriers is likely to alter the dynamic performance of a train further. However, few literatures focusing on the effect of noise barrier on the dynamic performance of a train in crosswind could be found. How the noise barrier affects the dynamic performance of trains has not been answered well yet, even though it is constructed based on the noise-related standards. To solve this problem has promoted the formation of this research. In this article, a three-dimensional (3-D) aerodynamic model based on the computational fluid dynamics (CFD), and a vehicle dynamics model of the train are developed (in section 2) to investigate the effect of the noise barrier on the flow field structure (in section 3) and the dynamic performance of train (in section 4) in crosswind.

2. Numerical models

A dynamic model is developed in this section by applying a 3-D aerodynamic model and a vehicle dynamics model together. The wind loads applied on the train surfaces can be extracted by simulation on the flow field structure with the 3-D aerodynamic model. Then the extracted wind loads are transformed to be the external forces and moments by linear interpolation for the train dynamic simulation based on the vehicle dynamics model. Finally, effects of the noise barrier on the flow field structure and train dynamic performance can be assessed with the aid of the 3-D aerodynamic model and the vehicle dynamics model which are going to be introduced in detail in the following subsections.

2.1 Aerodynamic model

CFD is an important method for investigation of train aerodynamics. Based on the practical application of noise barrier in Chinese high-speed railways, an aerodynamic model is established with the software package CFX.

2.1.1 Governing equations

In the aerodynamic model, the air is assumed to be viscous, incompressible, and isothermal. The RANS equations are employed with k-ε turbulence model based on Boussinesq hypothesis. The basic governing equations are as follows. More detailed descriptions of the equations can be found in reference (Versteeg and Malalasekera 1995).

The mass conservation equation is denoted as

$$\frac{\partial \rho}{\partial t} + \operatorname{div}\left(\rho \boldsymbol{u}\right) = 0 \tag{1}$$

where the symbol ρ is the air density, t is the time, div($\mathbf{A}$) is the divergence of the vector $\mathbf{A}$, $\boldsymbol{u}$ is velocity vector.

The momentum conservation equations are represented by

$$\frac{\partial(\rho u)}{\partial t}+\mathrm{div}(\rho u\boldsymbol{u})=\mathrm{div}(\mu\mathbf{grad}u)-\frac{\partial p}{\partial x}+S_u \tag{2}$$

$$\frac{\partial(\rho v)}{\partial t}+\mathrm{div}(\rho v\boldsymbol{u})=\mathrm{div}(\mu\mathbf{grad}v)-\frac{\partial p}{\partial y}+S_v \tag{3}$$

$$\frac{\partial(\rho w)}{\partial t}+\mathrm{div}(\rho w\boldsymbol{u})=\mathrm{div}(\mu\mathbf{grad}w)-\frac{\partial p}{\partial z}+S_w \tag{4}$$

where u, v, w denote successively the x, y, z components of the vector $\boldsymbol{u}$. μ is the air kinetic viscosity coefficient, **gran***f* (f=u, v, w) is the gradient of function f, p is the pressure, and S_u, S_v, S_w are the generalized source terms.

The energy conservation equation can be described as

$$\frac{\partial(\rho T)}{\partial t}+\mathrm{div}(\rho T\boldsymbol{u})=\mathrm{div}\left(\frac{k}{c_p}\mathbf{grad}T\right)+S_T \tag{5}$$

where T is the temperature, k is the heat transfer coefficient, S_T is the internal heat source of fluid. The relationship between T, ρ, and p are as follows

$$p=p(\rho,T) \tag{6}$$

The k-ε model includes two equations about turbulence kinetic energy and turbulence dissipation rate which are shown as follows

$$\frac{\partial}{\partial t}(\rho k)+\mathrm{div}(\rho\boldsymbol{u}k)=\mathrm{div}\left(\left(\mu+\frac{\mu_t}{\sigma_k}\right)\mathbf{grad}k\right)+G_k+\rho\varepsilon \tag{7}$$

$$\frac{\partial}{\partial t}(\rho\varepsilon)+\mathrm{div}(\rho\boldsymbol{u}\varepsilon)=\mathrm{div}\left(\left(\mu+\frac{\mu_t}{\sigma_\varepsilon}\right)\mathbf{grad}\varepsilon\right)+\frac{\varepsilon}{k}\left(C_{1\varepsilon}G_k-C_{2\varepsilon}\rho\varepsilon\right) \tag{8}$$

where μ_t is the turbulence viscosity coefficient, $\sigma_k/\sigma_\varepsilon$ are the corresponding Prandtl number of the turbulence kinetic energy and that of the turbulence dissipation rate, respectively. G_k is the generated term of turbulence kinetic energy, $C_{1\varepsilon}$ and $C_{2\varepsilon}$ are the empirical constants.

Eqs. (1)-(8) could be rewritten as a unified form as follows

$$\frac{\partial(\rho\varphi)}{\partial t}+\mathrm{div}(\rho\boldsymbol{u}\varphi)=\mathrm{div}(\Gamma\mathbf{grad}\varphi)+S \tag{9}$$

where φ is the generic variable, Γ is the generalized diffusion coefficient, S is the generalized source item, φ, Γ and S express the specific physical items in particular governing equation. Based on the Finite Volume Method (FVM), the governing equations are transformed to algebraic equations on grid nodes to perform numerical calculation.

2.1.2 Geometric model and computational domain

A 3-D geometric model of a Chinese CRH train running on an embankment with noise barriers is established to investigate the effect of noise barrier on the dynamic performance of high-speed trains. Some local features of the train such as pantograph, bogies, rails, sleepers, ballast are ignored in the geometric model for saving computational cost. Only the main structure and outline of the train and railway structure are reserved, and the surfaces of the train, track and ground are regarded as smooth. A CRH train generally consists of several motor cars and trailers with a total length of more than 200 m, where the shape of the head car and the tail car are the same, and the cross sections of middle cars are the same. Cooper (1979) found that the flow structure tends to be stable after the flow crosses over the head car, according to which the studied train model is simplified to be composed of a head car, a middle car and a tail car in this paper. And the basic dimensions of the simplified train are shown in Fig. 1.

The noise barrier geometry is based on a practical application in Chinese high-speed railway engineering. The schematic of the cross section of model and its geometric parameters are shown in Fig. 2. The track spacing is 5 m, the distance from central line of the track to that of the noise barrier is 4.65 m. The distance between embankment shoulder and the ground is 5 m, and the noise barrier height H counts from the embankment shoulder. The standard height is H = 2.95 m, i.e., the height of the noise barrier above the rail horizontal plane is 2.05 m. In this paper, uniform winds are applied. According to different positions of the train relative to the crosswind direction, two tracks are marked separately as the windward track and the leeward track.

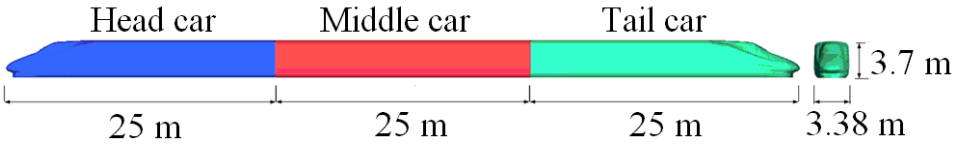

Fig. 1 Basic dimension of simplified high-speed train

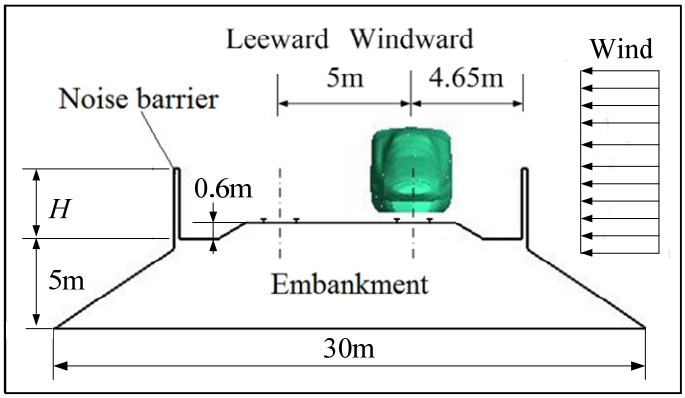

Fig. 2 Schematic of double-track embankment equipped with noise barrier

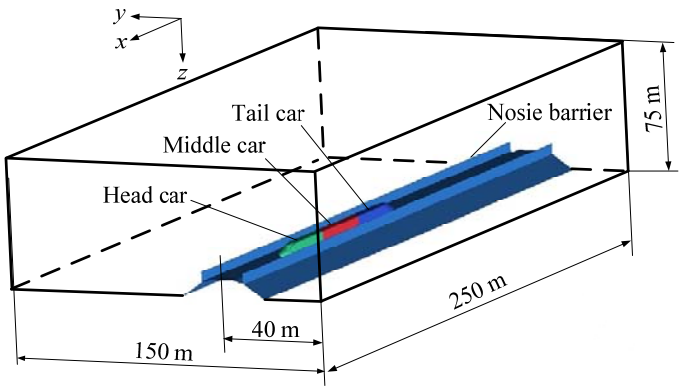

Fig. 3 Simulation domain and coordinate system

In crosswind condition, the flow field will change its structure and turbulence forms when it meets the train and railway structure. After a certain distance far from the train, the flow returns to be stable. Appropriate flow field area should be chosen to be big enough to ensure the fully development of the flow, while requiring as lower computational cost as possible. Through trial-and-error method, suitable computational domain is determined. The computational domain and the coordinate system are shown in Fig. 3 where an enough space is set after the tail car and the leeward track to ensure the fully development of the flow. The dimensions of the simulation domain are 250 m in x, 150 m in y and 75 m in z directions. The front and right sides of the simulation domain are set as inlet, and the back and left sides are designated as outlet. The top surface is set as an open boundary. The surfaces of the train, embankment, ground, and noise barrier are set to be the wall boundaries where the wall functions are applied to. The distance between the central line of the embankment and the right side inlet is 40 m, and that between the front side of the simulation domain and the head car nose is 60 m. The convergence criterion in the CFD calculation is given in the software by setting the residual type as RMS and the residual target as 1×10^{-5}, respectively.

2.1.3 Grid generation and boundary condition

Using tetrahedron elements and hexahedral prism elements, unstructured hybrid grids is generated in the finite volume of the flow field. The grids near the surfaces of the train, embankment and noise barrier are refined in order to satisfy the calculation accuracy of the boundary layers. Simultaneously, sparse grids are used far away from the carbody in order to reduce the number of the grid and improve the convergence rate. The local surface grids of the head car are displayed in Fig. 4. The grid space of the vehicle is controlled by the parameter named max size in the software. The max size is set as 0.12 m. The total number of the grids varies from 3 million to 4 million as the noise barrier height H changes.

In the simulation, the train is assumed to be stationary by applying a wind flow at a negative train running speed, namely the wind is flowing from the head to the tail cars. Additionally, the train is also encountering the crosswind. The inlet boundary condition is the resultant flow of the winds from front and side. The outlet boundary condition is designated with a relative pressure of 0 Pa.

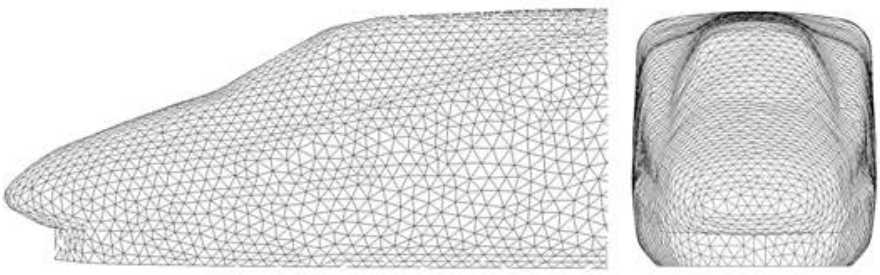

Fig. 4 Local grids of head car

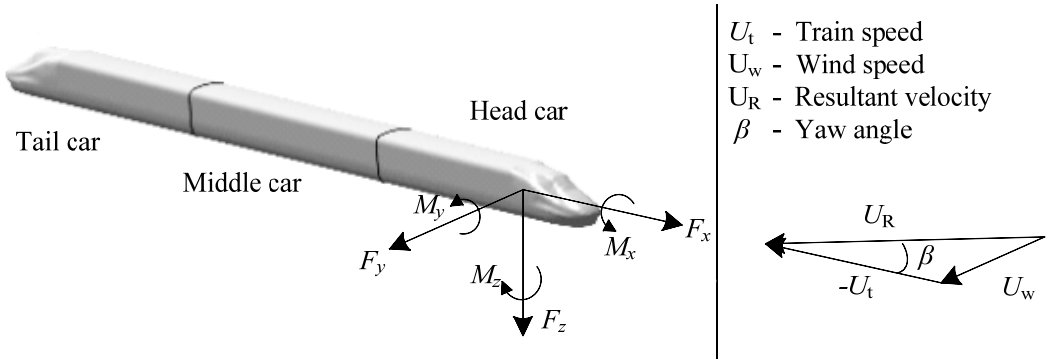

Fig. 5 Aerodynamic forces and moments

2.1.4 Aerodynamic forces and moments

In crosswind condition, effect of the wind on the train is through the action of the aerodynamic forces and moments extracted from the flow field simulation. For simplifying the calculation, the same coordinate system is used in the aerodynamic model and vehicle system dynamics model. The train speed is label as U_t along the $+x$ direction and the wind speed is U_w along the $+y$ direction. The pressure and shear stress on the train surfaces are transformed to the drag force (F_x), side force (F_y), and lift force (F_z) separately along x axis, y axis and z axis. It should be noted that, when F_z is negative, the direction of the vertical force is perpendicular to ground and upward, namely the 'lift force'. The resulted moments are the overturning moment (M_x), pitching moment (M_y), and yaw moment (M_z) corresponding to the x, y and z axis.

The aerodynamic forces and moments are applied to the centroid of the train. It could be added directly to the centroid of train in the vehicle system dynamics model under the benefit of the uniform coordinate system.

2.2 Vehicle system dynamics model

Based on multi-body dynamics, with aerodynamic forces and moments, equation of motion of the vehicle system is obtained as follows

$$\mathbf{M}\ddot{\mathbf{X}} + \mathbf{C}\dot{\mathbf{X}} + \mathbf{K}\mathbf{X} = \mathbf{P} + \mathbf{P}_w \tag{10}$$

where the symbols **M**, **C**, and **K** are the mass, damping and stiffness matrices respectively. $\mathbf{X}$, $\dot{\mathbf{X}}$ and $\ddot{\mathbf{X}}$ are the displacement, velocity and acceleration vectors respectively. **P** is the generalized load vector and $\mathbf{P}_w$ is the vector of wind loads.

The train dynamics model is established with the aid of the commercial software-SIMPACK. As mentioned afore, the train dynamics model is composed of three cars, i.e., the head car, the middle car and the tail car, which are shown in Fig. 6. Components of the train are regarded as rigid, and they are simplified into four wheelsets, eight axle boxes, two frames and one carbody. Each of the carbody, frame and wheelset has six degrees of freedom (DOFs), while the axle box has one DOF. And there are eight constraints between wheels and rails. Thus, there are totally 42 independent DOFs in a single vehicle. The middle car is linked with the head and the tail cars through spring-damper elements. The input forces and moments contain the side force, lift force, overturning moment, pitching moment and yaw moment. Track irregularity is also considered in the model. In this simulation, the German high-speed railway track irregularity is applied. The range of the track irregularity wavelength is 2~120 m.

3. Flow structure around high-speed train on embankment with railway noise barrier in crosswind

Effect of the noise barrier on the flow structure around train in crosswind is analysed in this section, and the flow characteristics with and without noise barrier are compared to demonstrate the effect.

3.1 Flow structure around train on windward track

Fig. 7 presents the flow structure around the train running on the windward track without (left column) and with (right column) noise barrier in crosswind. The wind blows from the right to the left at a speed of 15 m/s, and train speed is 300 km/h.

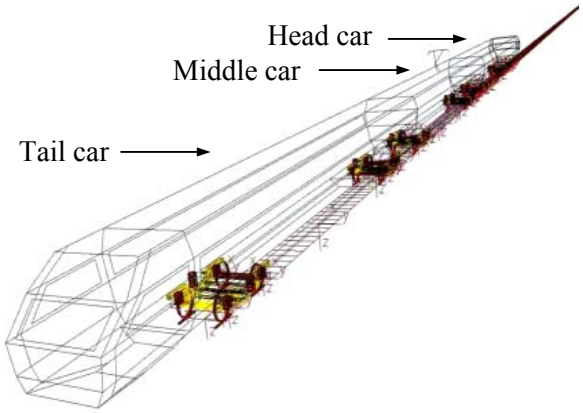

Fig. 6 Vehicle system dynamics model in SIMPACK

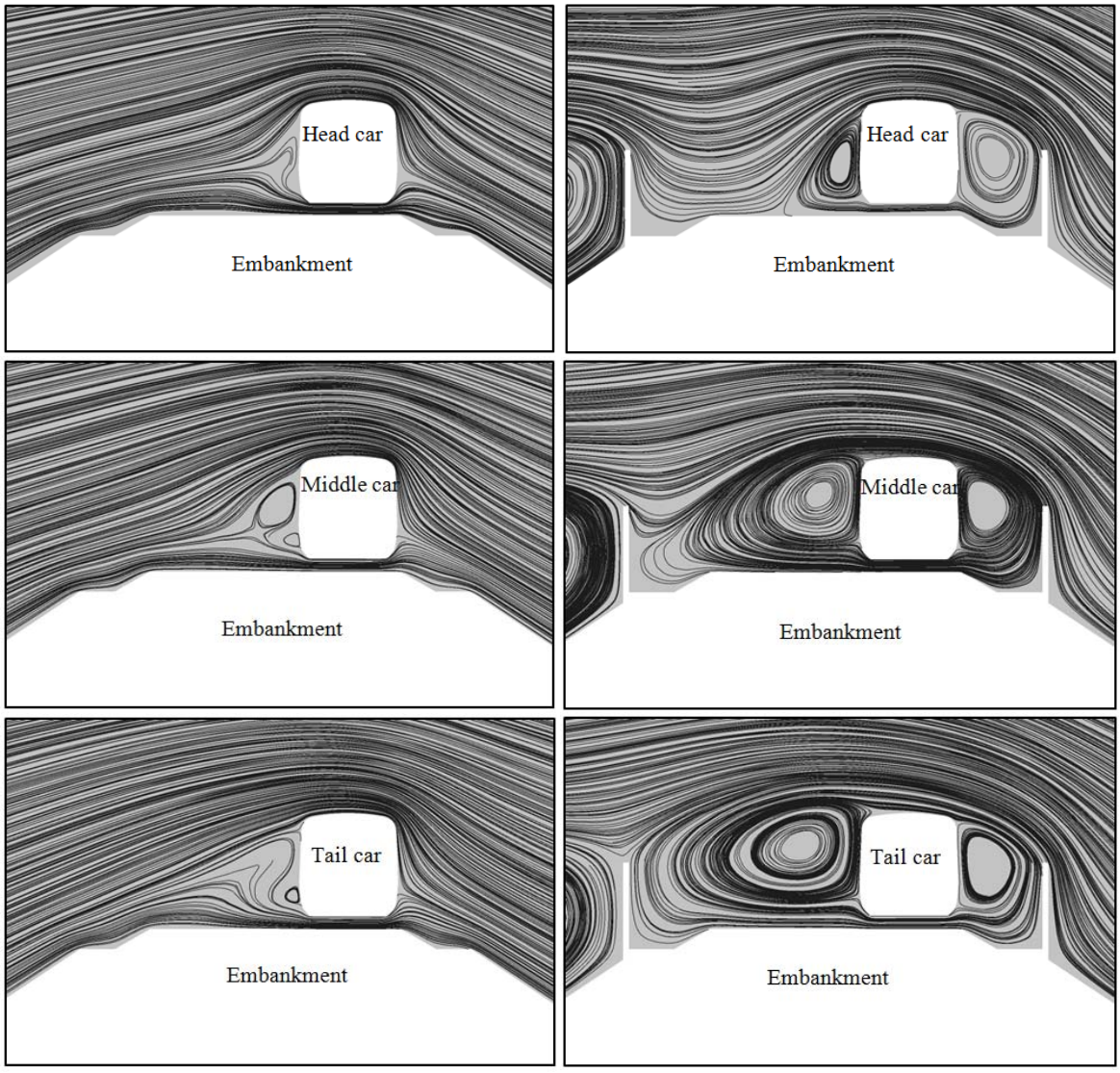

(a) Without noise barrier (b) With noise barrier

Fig. 7 Flow structure around train on windward track (wind blows from the right to the left)

It can be seen in Fig. 7 that the wind blows directly on the windward side surfaces of the train, and then is split to two parts in the case without noise barrier. One runs across the top of the train, and the other flows across the bottom of the train. Vortexes are formed behind the train on the leeward side of the train, which may produce negative pressure area. Due to the existence of the yaw angle between the resultant flow and the train, the vortexes forming on the leeward side of the train get larger at a further position far away from the head car, i.e., the vortex behind the head car is the smallest, and that behind the tail car is the biggest. The flows behind the middle and tail cars are separated more seriously than that behind the head car. It can be observed clearly that two vortexes (up and down) are gradually formed behind the middle and tail cars. The direct impact of

the coming flow on the train and the negative pressure area formed behind the train are able to contribute to the increase of the lateral aerodynamic forces and moments acting on the train running on embankment without noise barrier.

After setting up the noise barrier on the embankment, the crosswind flow meets the noise barrier firstly and it is lifted then toward to the upward of the train, which makes an increase of the flow speed near the top of the train. Due to the effect of the noise barrier, some relative semi-closed areas are formed between the train and noise barrier, resulting in the vortexes developed on both sides of the train. The flow field structure with noise barriers is obviously different from the cases without noise barriers. In the case without noise barriers, nearly no vortex is formed on the windward side of the train, while the vortex areas formed on the leeward side of the train are relatively small. In the case with noise barriers, there are some vortexes formed on the windward side of the train, and the vortex areas formed on the leeward side are relatively larger than that without noise barriers. Because of the protective action of the noise barrier, the impact of the crosswind flow on the train is weakened. However, the lateral forces induced by the pressure differences caused by the vortexes formed on both sides of the train gradually play a major role in the aerodynamic performance of the train. For example, the pressure difference formed on the two sides of the head car may lead to a resultant lateral force whose direction is opposite to the wind flow. Among the vortexes formed behind the train with noise barriers, the one behind the head car is the smallest and that behind the tail car is the biggest.

3.2 Flow structure around train on leeward track

The crosswind flow, sometimes, from the noise barrier at the windward side to that at the leeward side, such as the crosswind defined in subsection 3.1, while it is likely to change its direction to be reversed in some other cases. The flow structure around train running on the leeward track without (left column) and with (right column) noise barriers in crosswind is represented in Fig. 8 where the wind blows from the right to left. For comparison with the case of the windward track, the same wind speed of 15 m/s and the same train speed of 300 km/h are employed here.

In Fig. 8, in the case without noise barriers, the coming flow blows directly on the windward side of the train, and the flow structure around the train on the leeward track is similar to that on the windward track. While after setting up the noise barriers, vortexes are also formed on both sides of the train on the leeward track. The vortex areas formed on the windward side of the train appear to be larger than that when the train is on the windward track due to the truth that the space between the train and the noise barrier on the windward side is larger. Negative pressure areas are formed on the windward side of the train. The lateral force induced by the pressure difference of the vortexes and the lateral force due to the friction between the flow and the surface of the train will lead to a resultant lateral force which is opposite to the wind direction. In the case of the leeward case, the coming flow is lifted firstly by the noise barrier, and then goes down a little after passing the windward track and gets impact with the train. The protective effect of the noise barrier in crosswind for the train on the leeward track may be less obvious than on the windward track.

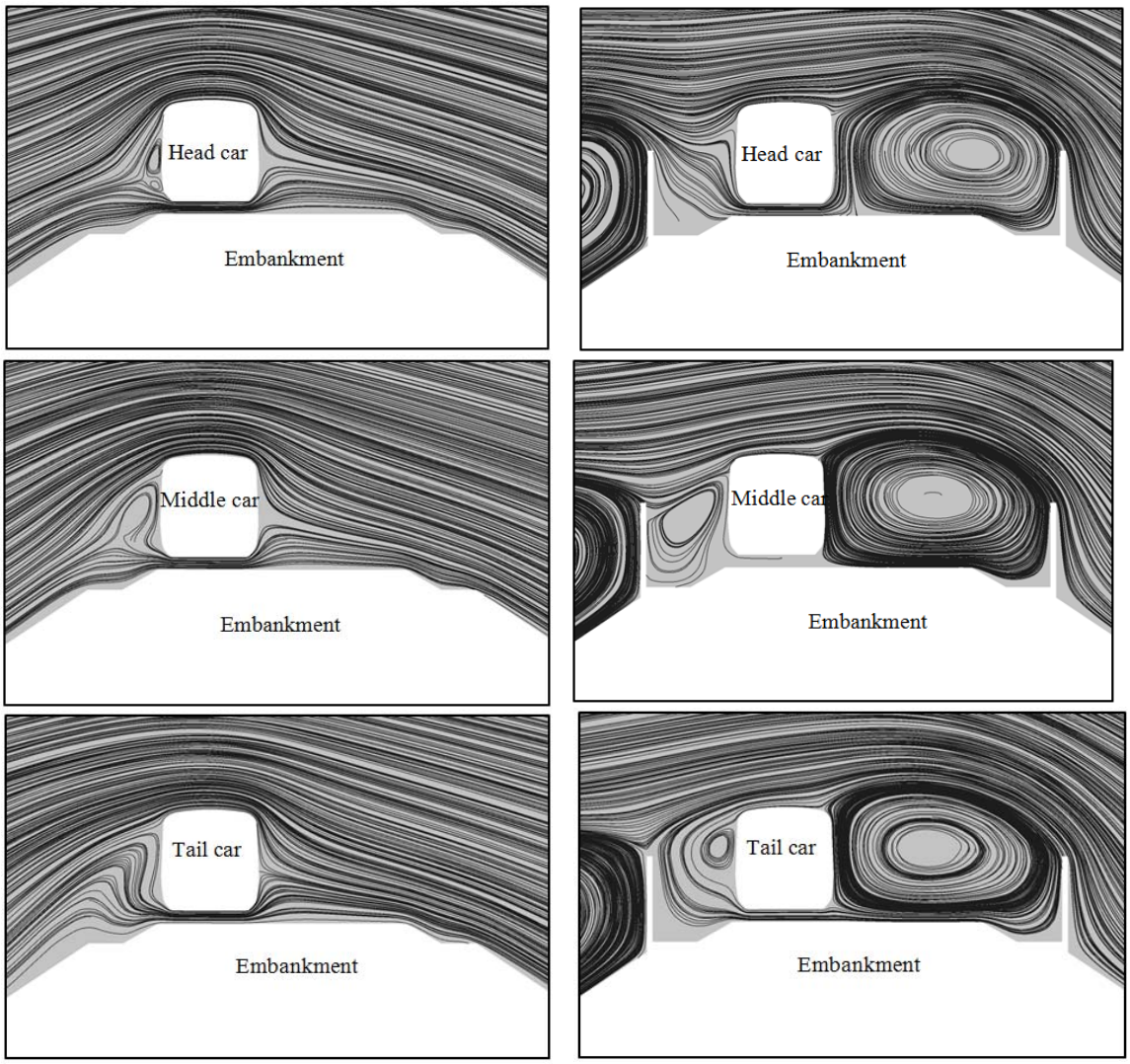

(a) Without noise barrier (b) With noise barrier

Fig. 8 Flow structure around train on leeward track (wind blows from the right to the left)

4. Dynamic performance of high-speed train influenced by noise barrier in crosswind

Based on the analysis in section 3, the flow field structure around the train is affected greatly by the noise barrier, where the dynamic lateral forces and moments are also changed, thus it is likely to change the dynamic performance of the train. This section is aiming at investigating the effect of the noise barrier on the dynamic performance of the train in crosswind. Some dynamic indexes of a high-speed train running on an embankment with and without noise barriers in crosswind are compared, based on which the optimized height of the noise barrier is suggested. The dynamic

indexes include the derailment coefficient Q/P, the wheel unloading rate $\Delta P / \overline{P}$ and the overturning coefficient P_{d} / P_0. Here, the symbols Q and P indicate the lateral and vertical wheel–rail forces, ΔP and $\overline{P}$ represent the value of the wheel unloading and the mean static wheel load, and P_{d} and P_0 are the vertical dynamic load for a single side wheel and the corresponding vertical static load, respectively. For Chinese high-speed railway vehicles, the following limits are usually employed: $Q/P \leq 0.8$, $\Delta P / \overline{P} \leq 0.8$, and $P_{\mathrm{d}} / P_0 \leq 0.8$.

4.1 Dynamic performance of train on windward track

The dynamic indexes of the head car, middle car and tail car on windward track with and without noise barrier in crosswind are listed in Table 1. The same working condition is applied here, namely the wind speed is 15 m/s and the train speed is 300 km/h.

It can be seen from Table 1 that indexes of both the head car and the tail car with the noise barriers become decreased compared with that without noise barriers. The noise barriers not only reduce the noise, but also improve the running performance of the head car in crosswind.

In the case without noise barrier, the dynamic performance of the middle car is better than that of the head car and the tail car. After setting up noise barriers, the dynamic performance of the middle car has not been significantly improved. What's more, the derailment coefficient, the vertical wheel–rail force and the lateral wheelset force of the middle car are even larger than the case without noise barriers. In the case with noise barriers, all the indexes except the lateral wheel–rail force of the middle car are larger than that of the head car. Being completely opposite to the case without noise barriers, the running performance of the middle car is worse than the head car in the case with noise barrier.

The dynamic performance of the tail car is better than the head car, but worse than the middle car when without noise barriers. After setting up noise barriers, the indexes of the tail car are decreased, and its running performance is very close to the head car but a little better than the middle car.

Table 1 Dynamic indexes of train on windward track with and without noise barrier

Car	With noise barrier or not	Derailment coefficient	Wheel unloading rate	Overturning coefficient	Lateral wheel–rail force (kN)	Vertical wheel–rail force (kN)	Lateral wheelset force (kN)
Head car	No	0.250	0.737	0.424	26.87	118.70	36.01
	Yes	0.121	0.407	0.173	8.81	94.60	15.55
Middle car	No	0.119	0.474	0.240	9.04	86.891	15.54
	Yes	0.134	0.417	0.232	8.74	98.950	15.69
Tail car	No	0.151	0.528	0.305	9.68	99.70	17.48
	Yes	0.125	0.400	0.200	8.77	88.57	15.84

It can be also seen that the dynamic performance of the head car is no longer obviously worse than the middle car and tail car after setting up noise barriers. This is related to the protective role of the noise barriers. Without noise barrier, the crosswind are lifted along the embankment, and then meet the head car at first, which results in the worst running performance of the head car. After setting up noise barriers, the head car no longer suffers directly the impact from the flow, which will make the differences of dynamic indexes between the cars be less obvious than the case without noise barriers.

4.2 Dynamic performance of train on leeward track

The dynamic indexes of the head car, middle car and tail car on leeward track with and without noise barrier in crosswind are represented in Table 2. Again, the wind speed of 15 m/s and the train speed of 300 km/h are employed.

In Table 2, the indexes of the head car on the leeward track are decreased when setting up noise barrier. The dynamic performance of the middle car is better than the head car in the case without noise barriers. After setting up the noise barriers, the dynamic performance of the middle car has not been significantly improved, and its derailment coefficient and wheel rail vertical force are larger than the case without noise barrier. Additionally, the derailment coefficient and overturning coefficient of the middle car are larger than the head car, which is also different from the case without noise barrier.

For the tail car, the dynamic indexes are smaller than the head car when without noise barriers. While after setting up the noise barriers, these indexes are very close to those without noise barriers, which indicates the running performance of the tail car has not been obviously improved. Another noticeable result could be observed that these indexes of the tail car are larger than the middle car, and some of them are even larger than the head car.

In the case of the train on the leeward track with a relatively larger space between the windward noise barrier and the train, it can be concluded that the coming flow will go down after it passes the noise barrier, which causes that a part of the flow will directly impact on the train. Consequently, the protective role of the noise barrier on the dynamic performance of the train on the leeward track is less obvious than that on the windward track. Thus, the running safety of the train on the leeward track is generally worse than on the windward track.

Table 2 Dynamic indexes of train on leeward track with and without noise barrier

Car	With noise barrier or not	Derailment coefficient	Wheel unloading rate	Overturning coefficient	Lateral wheel–rail force (kN)	Vertical wheel–rail force (kN)	Lateral wheelset force (kN)
Head car	No	0.257	0.753	0.444	27.26	121.62	37.53
	Yes	0.126	0.443	0.180	10.40	96.42	17.63
Middle car	No	0.127	0.528	0.286	9.97	92.700	16.23
	Yes	0.134	0.411	0.230	8.79	97.195	16.03
Tail car	No	0.139	0.490	0.250	9.38	98.48	16.60
	Yes	0.146	0.433	0.250	9.02	98.78	16.36

4.3 Effect of noise barrier height on dynamic performances

It can be predicted that the height of the noise barrier is one of the key parameters determining the flow field structure around the train, thus influencing the dynamic performance of the train. This subsection is focusing on exploring the influence of noise barrier height on the train dynamic performance. The running performances of the train on the windward track and on the leeward track are also compared through the maximum dynamic indexes of the train. Variations of the derailment coefficient, wheel unloading rate and overturning coefficient of the train running on the windward track and on the leeward track with different noise barrier height are illustrated in Fig. 9. The speed of the wind is also 15 m/s, and the speed of the train 300 km/h. The heights of the noise barrier H are set successively as 0 m, 2 m, 2.5 m, 2.95 m (standard height), 3.2 m, 3.45 m, 3.7 m, 3.95 m and 4.5 m. The standard height (2.95 m) indicates the value of the noise barrier height employed in the practical engineering of the CRH line analysed in this paper.

It can be seen from Fig. 9 that all the dynamic indexes of the train equipped with noise barriers are smaller than those without noise barrier. The running performance of the train on the windward track is better than on the leeward track. The dynamic indexes decrease with the increase of the noise barrier height before the height is up to a value, however, when the height is above this value, the indexes will become increasing with growth of the height. For the case that the train is running on the windward track, the indexes for the train appear to be the smallest when the noise barrier height lies in a region between 2.5 m and 2.9 m. However, this region will move to be between 2.95 m and 3.2 m for the case on the leeward track. It is interesting that these results enable the possible optimization of the noise barrier height. A special attention should be paid to that the standard height of the noise barrier, namely H=2.95 m, is very close to the two regions aforementioned, which means the noise barrier height employed in the CRH line studied in this paper is reasonable. However, when H is larger than 3 m, the indexes of the train will increase gradually with increase of the height, which means that a noise barrier height above 3 m is not suggested. These results could supply the theoretical guidance on the selection of proper noise barrier height at the view point of better flow field structure and train dynamic performance.

5. Conclusions

On the basis of the analysis and discussion on the numerical results, it can be concluded that:

(1) Existence of the noise barrier on high-speed railways will change the flow structure around a train in crosswind. The noise barrier could change structure of the wind and decrease the direct impact of the flow on the train. Vortexes are formed on both sides of the train in the case with noise barrier. The negative pressure areas forming on the windward side of the train may lead to a resultant lateral force applied on the train with the opposite direction of the crosswind, making the train tend to overturn.

(2) In crosswind, the dynamic performance of the high-speed train running on an embankment with noise barriers is better than the case without noise barriers.

(3) Without noise barrier, the head car is most affected by the crosswind and its dynamic performance is the worst. While after setting up noise barriers, dynamic performance of the head car becomes better obviously due to that it no longer suffers the direct impact of the crosswind. Although the impact from the wind on the middle car and tail car decreases too, the lateral force induced by the pressure difference between the vortexes increases, which leads to a phenomenon

that some indexes of the middle car and tail car are larger than the head car, some are even larger than the case without noise barrier.

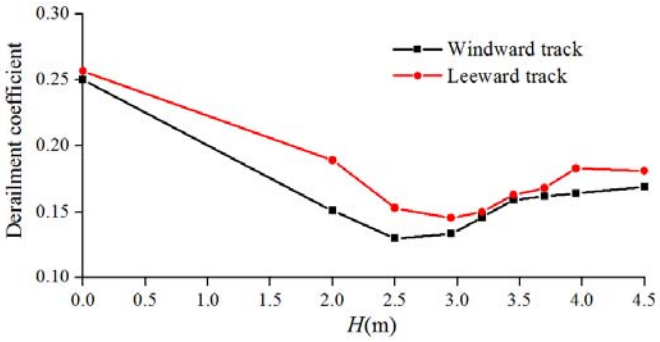

(a) Derailment coefficient

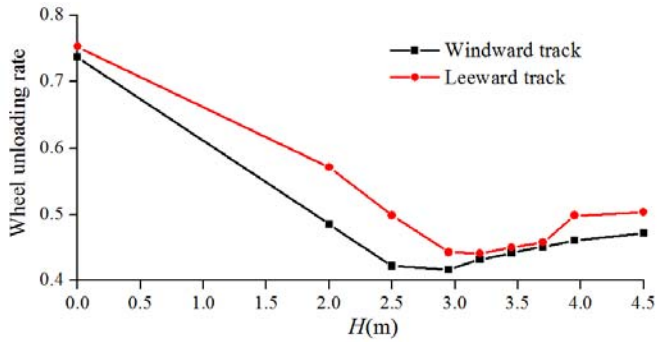

(b) Wheel unloading rate

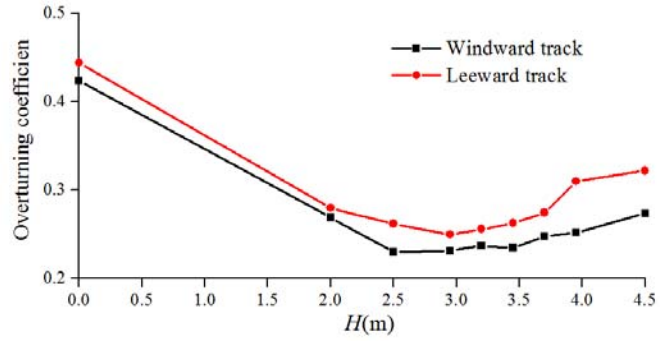

(c) Overturning coefficient

Fig. 9 Dynamic indexes with different noise barrier height

(4) For different noise barrier height, the running performance of high-speed trains on the windward track is always better than on the leeward track. The noise barrier heights for the minimized indexes indicating the best train dynamic performance exist, which supplies the possibility for optimization on the noise barrier height. And a noise barrier with an excessive height is not advised to be employed.

(5) The noise barrier with the standard height of 2.95 m used in present CRH line analysed in this paper is objectively reasonable from the view point of flow field structure and train dynamic performance.

Acknowledgements

This work was supported by the National Key Basic Research Program of China (973 Program) under Grant No. 2013CB036206, and the National Natural Science Foundation of China under Grant No. 50838006.

References

Baker, C.J. (1991), "Ground vehicles in high cross winds. Part I: steady aerodynamic forces", *J. Fluid. Struct.*, **5**(1), 69-90.

Cooper, R.K. (1979), "The effect of cross-wind on trains", *Proceedings of the Aerodynamics of Transportation, ASME-CSME Conference*,18-20 June, Niagara.

Diedrichs, B., Sima, M., Orellano, A. and Tengstrand, H. (2007), "Crosswind stability of a high-speed train on a high embankment", *J. Rail Rapid Transit*, **221**(2), 205-225.

Gilbert, T., Baker, C. and Quinn, A. (2013), "Aerodynamic pressures around high-speed trains: the transition from unconfined to enclosed spaces", *J. Rail Rapid Transit*, **227**(6), 608-62.

Guo, W.W., Xia, H. and Zhang, N. (2013), "Dynamic responses of Tsing Ma Bridge and running safety of trains subjected to Typhoon York", *Int. J. Rail Transportation*, **1**(3), 181-192.

Hemida, H. (2006), *Large-eddy simulation of the flow around simplified high-speed trains under side wind conditions*, Ph.D. Dissertation, Chalmers University of Technology, Göteborg, Sweden.

Herbsta, A.H., Mulda, T.W. and Efraimsson, G. (2014), "Aerodynamic prediction tools for high-speed trains", *Int. J. Rail Transportation*, **2**(1), 50-58.

Khier, W., Breuer, M. and Durst, F. (2000), "Flow structure around trains under side wind conditions: a numerical study", *Comput. Fluids*, **29**(2), 179-195.

Khier, W., Breuer, M. and Durst, F. (2002), *Numerical computation of 3D turbulent flow around high-speed trains under side wind conditions*, TRANSAERO – a European initiative on transient aerodynamics for railway system optimization, Springer-Verlag.

Li, Y. and Tian, H. (2012), "Lateral aerodynamic performance and speed limits of double-deck container vehicles with different structures", *J. Cent. South. Univ.*, **19**(7), 2061-2066.

Li, Y., Hu, P., Xu, Y., Zhang, M. and Liao, H. (2014), "Wind loads on a moving vehicle–bridge deck system by wind-tunnel model test", *Wind Struct.*, **19**(2), 145-167.

Luo, J. and Yang, Z. (2010), "Research on the noise barrier height change of the monoline viaduct affecting the aerodynamic characteristic of high speed train", *IEEE Computer Society, 2010 International Conference of Intelligent Computation Technology & Automation, Changsha*.

Rezvani, M.A. and Mohebbi, M. (2014), "Numerical calculations of aerodynamic performance for ATM train at crosswind conditions", *Wind Struct.*, **18**(5), 529-548.

Sun, X., Wang, B., Gong, M., Ding, S. and Tian, A. (2013), "Study on the safety of high-speed trains under crosswind", *Adv. Inform. Sci. Service Sci.*, **5**(1), 582-588.

Versteeg, H.K. and Malalasekera, W. (1995), *An introduction to computational fluid dynamics: the finite volume method*, England: Longman Group Ltd.
Xia, H., Guo, W.W., Zhang, N. and Sun, G.J. (2008), "Dynamic analysis of a train-bridge system under wind action", *Comput. Struct.*, **86**(19-20), 1845-1855.
Zhang, T., Xia, H. and Guo, W.W. (2013), "Analysis on running safety of train on bridge with wind barriers subjected to cross wind", *Wind Struct*., **17**(2), 203-225.

CC